Elastic constants and dimensions of imprinted polymeric nanolines determined from Brillouin light scattering*

W L Johnson[1], S A Kim[1], R Geiss[1], C M Flannery[1], C L Soles[2], C Wang[2], C M Stafford[2], W-L Wu[2], J M Torres[3], B D Vogt[3] and P R Heyliger[4]

[1] Materials Reliability Division, National Institute of Standards and Technology, 325 Broadway, Boulder, CO 80305, USA

[2] Polymers Division, National Institute of Standards and Technology, 100 Bureau Drive, Gaithersburg, MD 20899, USA

[3] Flexible Display Center, Arizona State University, Tempe, AZ 85284, USA

[4] Department of Civil and Environmental Engineering, Colorado State University, Fort Collins, CO 80525, USA

Abstract

Elastic constants and cross-sectional dimensions of imprinted nanolines of poly(methyl methacrylate) (PMMA) on silicon substrates are determined nondestructively from finite-element inversion analysis of dispersion curves of hypersonic acoustic modes of these nanolines measured with Brillouin light scattering. The results for the cross-sectional dimensions, under the simplifying assumption of vertical sides and a semicircular top, are found to be consistent with dimensions determined from critical-dimension small-angle x-ray scattering measurements. The elastic constants C_{11} and C_{44} are found to be, respectively, 11.6% and 3.1% lower than their corresponding values for bulk PMMA. This result is consistent with the dimensional dependence of the quasi-static Young's modulus determined from buckling measurements on PMMA films with lower molecular weights. This study provides the first evidence of size-dependent effects on hypersonic elastic properties of polymers.

(Some figures in this article are in colour only in the electronic version)

1. Introduction

Implementation of nanoimprint lithography as a reliable technique for nanoscale patterning of thin films depends on the development of methods for modeling and controlling the mechanics of embossing at elevated temperatures, cooling to ambient temperatures, and removal of imprints from the mold [1]. A lack of information on elastic constants (stiffness coefficients) and viscosity as a function of temperature is a significant obstacle to this development, because of the inability of conventional measurement techniques to accurately determine these properties in structures with more than one nanoscale dimension [2]. The importance of developing metrology that is effective at the nanoscale is most pressing in the case of polymeric imprints, because significant deviations from bulk properties are expected when one or more dimensions approach the scale of the macromolecular diameters (typically, several tens of nanometers) [3, 4]. In this work, we present methods for determining the stiffness coefficients and dimensions of polymeric nanolines from inversion analysis of Brillouin-light-scattering (BLS) [5] measurements of vibrational spectra.

Hartschuh *et al* [6] demonstrated that vibrational modes in photolithographically patterned nanolines can be detected in BLS spectra and suggested that such measurements could provide a basis for determining the elastic stiffnesses.

1

In subsequent work on photolithographically patterned [7] and imprinted [8] polymeric nanolines, the symmetries of the displacements of the three lowest-frequency vibrational modes were determined through comparison of the measured dispersion curves with finite-element (FE) and Farnell–Adler [9] calculations. The lowest-frequency peak in the BLS spectra arises from a flexural mode with transverse displacements primarily parallel to the surface of the substrate. The second and third peaks arise from modes similar to Rayleigh and Sezawa modes of blanket films [10] (referred to here as Rayleigh-like and Sezawa-like), with displacements primarily perpendicular to the substrate.

Inversion analysis of BLS spectra from imprinted poly(methyl methacrylate) (PMMA) nanolines was pursued by Johnson *et al* [8] using Farnell–Adler models. One conclusion of that work was that relatively poor fitting of the calculations to the BLS data can be attributed to inaccuracy of the gross approximation of a blanket film in the Farnell–Adler models for the Rayleigh-like and Sezawa-like modes of the nanolines. For example, very different dimensional and stiffness parameters were extracted from fits with and without the Sezawa-like mode included. Johnson *et al* [8] suggested that FE methods could overcome this problem to provide more accurate nanoline parameters.

Heyliger *et al* [11] presented a detailed description of the FE method for modeling vibrational modes of nanolines, performed calculations for rectangular and rounded-top cross sections, determined the form of additional vibrational modes, and evaluated the accuracy and range of validity of the approximations that were employed. A higher-order flexural mode, not detected in BLS measurements, was found to have a dispersion curve close to that of the Rayleigh-like mode. Dispersion curves above the first Sezawa-like mode were identified with higher-order Sezawa-like and flexural modes.

Inversion of BLS data from an array of imprinted PMMA nanolines is performed here using the FE approach of Heyliger *et al* [11], which enables an arbitrary cross-sectional geometry to be incorporated in the model. Information on the dimensions of the nanolines is simultaneously determined under the simplifying assumption of a cross-sectional shape with only two adjustable parameters. To provide independent information on nanoline dimensions, critical-dimension small-angle x-ray scattering (CD-SAXS) measurements and analysis were performed. Quasi-static buckling measurements on PMMA films with a lower molecular weight were also used for comparison with elastic stiffness coefficients determined from BLS/FE.

2. Specimen

The samples in this work were imprinted PMMA line gratings with a polymer molecular weight of 950 kg mol^{-1}. The mold was silica that was patterned and etched using 193 nm deep-UV lithography. The surface of the silica mold was treated with fluorinated trichlorosilane to generate a low-energy surface that facilitated pattern release. The mold was pressed into a PMMA film with a thickness of ~300 nm at 180 °C for 10 min under a pressure of 8 MPa in vacuum to generate the imprints on a (100) silicon surface. The initial imprinted lines were trapezoidal in cross section with an average linewidth of approximately 101 nm, height of 170 nm, periodicity of 364 nm, length of 10 μm, and average sidewall angle of 4.2°. Multiple sets of lines were arranged with a spacing of 1 μm between their ends. After imprinting, there was also a PMMA residual layer approximately 100 nm thick beneath the imprinted line gratings. This residual layer was removed with an O$_2$ plasma etch at a pressure of 0.7 Pa (5 mTorr), 80 W, etch time of 110 s, and O$_2$ flow rate of 12 standard cubic centimeters per minute (sccm). The PMMA etch rate under these conditions was 56 nm min^{-1}.

In addition to removing the residual layer, the plasma etch modified the widths, heights, and shape of the nanolines. Figure 1 shows field-emission scanning-electron-microscope (FESEM) images of the imprinted PMMA after the residual layer was removed. These images were obtained with an incident electron beam energy of 500 V, which is low enough to avoid evaporation of the PMMA. The lower image (figure 1(b)) was obtained with an incident SEM beam angle of 82.5° relative to the normal of the specimen. At this high angle, the 10 μm lengths of the nanolines appear very foreshortened and geometric irregularities are accentuated. To reduce charge accumulation and associated blurring and distortion during acquisition of the image in figure 1(b), a few monolayers of carbon were deposited on the specimen after BLS and CD-SAXS measurements were completed.

Only incomplete information on the cross-sectional geometry of the nanolines is provided by the image of figure 1(b). The tops are clearly rounded as a result of the plasma etching. However, the degree to which the sides are nonparallel is difficult to assess from the image. As described below, CD-SAXS was used to provide additional information about tilting of the sides of the nanolines. Information on the cross-sectional geometry was also sought from FESEM of a cleaved section of the specimen, but this measurement was unsuccessful because of apparent plastic deformation of the nanolines during cleaving and more severe effects of charge accumulation on the image. Similar problems with charge accumulation in SEM measurements of nanopatterned polymers are commonly encountered by other researchers [12]. Even in the absence of charging effects, accurate determination of the dimensions and shape of nanopatterned polymers with SEM is a challenging multiparameter problem [13].

3. Methods

3.1. Brillouin light scattering

BLS measurements were performed at a wavelength of 532 nm in a 180° backscattering configuration (with the incident laser beam coincident with the axis of the lens that collects the inelastically scattered light) [5]. The normal of the Si substrate was tilted at an angle θ relative to the incident beam. The principal (long) axis of the nanolines was in the plane that is defined by the incident beam axis and the normal of the
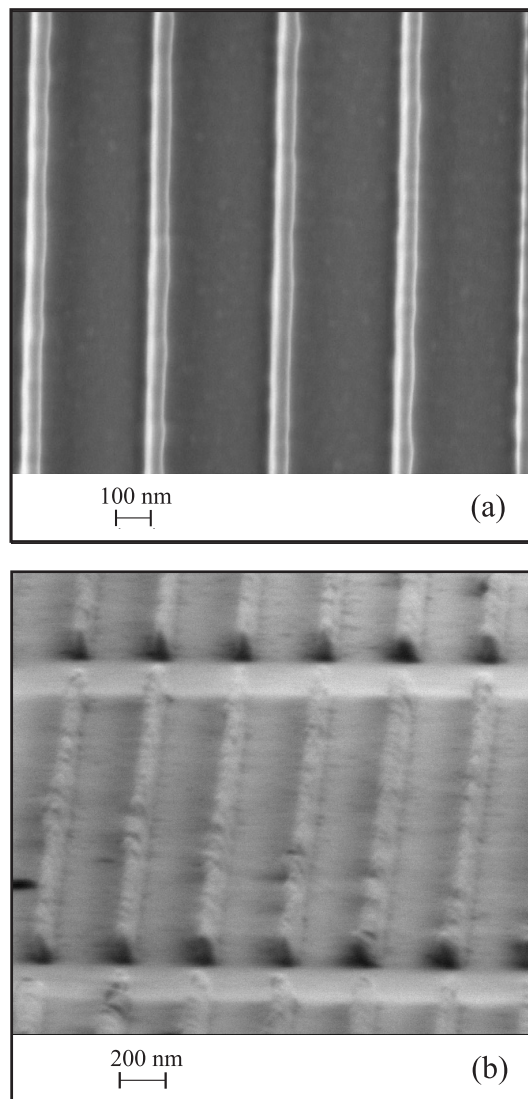
Figure 1. FESEM images of the imprinted PMMA nanolines.
(a) Incident electron beam parallel to the specimen normal.
(b) Incident electron beam tilted 82.5° relative to the specimen normal.

substrate. The polarization of the incident light was also in this plane ('p polarized'). Inelastically scattered light from the specimen was passed without polarization filtering through an $f/1.2$ collection lens to a scanning $(3 + 3)$-pass tandem Fabry–Perot interferometer [14]. Photons transmitted through the interferometer were detected by a photomultiplier, and counts from the photomultiplier were accumulated in a multichannel analyzer as a function of the scanned mirror spacing and corresponding frequency shift of the light.

The value of θ was varied to select the wavevector of detected acoustic modes propagating along the lengths of the nanolines. Because the height of the nanolines is significantly less than the wavelength of the incident light, the Bragg condition for constructively backscattered light from modes localized in the nanolines breaks down with respect to phase variation parallel to the substrate normal, and only the Bragg condition for components of the wavevectors parallel to the

surface remains. Therefore, for backscattered light coincident with the axis of the collection lens, the detected acoustic wavenumber q_0 along the principal nanoline axis is given by the usual BLS relation for surface waves on opaque planar surfaces [5],

$$q_0 = \pm \frac{4\pi}{\lambda_0} \sin \theta, \qquad (1)$$

where λ_0 is the wavelength of the incident light. From this equation, values of $|q_0|$ in our measurements were in the range of 13.5–22.8 μm^{-1}, corresponding to the selected range of 35°–75° for θ.

The non-zero diameter of the collection lens leads to a finite range of collection angles and, in general, a corresponding shift in the average wavenumber of detected acoustic waves, relative to that given by equation (1). To correct for this effect, we used the analytical procedure of Stoddart *et al* [15], not including any angular dependence of the surface reflectivity or acousto-optic coupling coefficients. Differences between the corrected wavenumbers q and uncorrected wavenumbers q_0 are in the range of 1.0%–1.4%.

3.2. Finite-element methods

We employed the finite-element methods of Heyliger *et al* [11] to model the displacement patterns and dispersion curves of the vibrational modes of the nanolines. In this approach, the displacements are approximated as varying sinusoidally in phase along the length, and the nanoline/substrate interface is approximated as rigid. These approximations were found by Heyliger *et al* to be valid for the lowest flexural, Rayleigh-like, and lowest three Sezawa-like modes over specified ranges of wavenumbers.

3.3. CD-SAXS

Information on nanoline geometry and dimensions was obtained from CD-SAXS, in addition to FESEM. CD-SAXS has previously been applied successfully to measure the critical dimensions in nanoscale patterns, including the pitch, average cross-sectional width, height, and sidewall angles of line gratings ranging from 10 to 500 nm in width [16, 17]. In CD-SAXS measurements, the diffracted intensity of a collimated x-ray beam is recorded on a two-dimensional detector as the beam passes through a periodic test structure. The observed intensity distribution is the square of the amplitude of the three-dimensional Fourier transform of the pattern and can be analyzed as a function of scattering angle to quantify the shape of the average pattern cross section as well as the variance in its dimensions in the scattering volume. Dimensional information along the thickness direction of the patterns is obtained by collecting scattering data at various angles of incidence. Further details on the CD-SAXS procedure and data analysis are provided elsewhere [18].

CD-SAXS data on the imprinted PMMA gratings in this study were collected at the 5-ID-DND beamline at the Advanced Photon Source of Argonne National Laboratory.
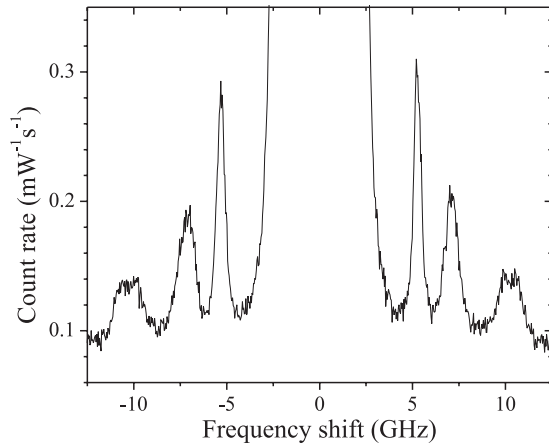
Figure 2. BLS spectrum acquired with $\theta = 60°$, corresponding to $q = 20.2 \ \mu m^{-1}$.

The x-ray energy was 17 keV. Scattered x-rays were collected on a CCD array with a sample-to-detector distance of 719.3 ± 0.5 cm.

4. Results

4.1. BLS

Figure 2 shows a representative BLS spectrum up to 12.5 GHz acquired with $\theta = 60°$, which corresponds to $q = 20.2 \ \mu m^{-1}$ for the detected acoustic modes. The large central peak, which arises from light that is reflected from the specimen with no change in frequency, obscures a peak near 2.6 GHz that is more clearly seen when the spectrometer is configured to scan over a smaller range of frequencies.

Values for the magnitude of the optical frequency shifts of the peaks in figure 2 (corresponding to the frequencies of the inelastically scattering acoustic modes) and those in spectra obtained at other values of θ were determined by fitting the peaks to Lorentzian functions. The highest-frequency peak in figure 2 was assumed to be a superposition of two closely spaced peaks and was fit to a sum of two Lorentzians. Figure 3 shows the acoustic mode frequencies determined from this analysis as a function of acoustic wavenumber q.

To provide initial input parameters for inversion analysis of the BLS data of figure 3, measurements of bulk longitudinal and Rayleigh waves were performed on a plate of PMMA with a thickness of approximately 17 μm. The starting material for fabricating this plate was the same as that for the imprinted nanolines. From these measurements, the longitudinal velocity v_1 and shear velocity v_2 were determined to be 2778 ± 10 and 1354 ± 10 m s^{-1}, using a value of 1.493 [19] for the index of refraction of PMMA at 532 nm. The density of bulk PMMA produced from different starting material was determined by Archimedes' method to be 1187 kg m^{-3}. The corresponding elastic stiffness coefficients, determined from the relations $C_{11} = \rho v_1^2$ and $C_{44} = \rho v_2^2$ for isotropic material, are $C_{11} = 9.161 \pm 0.047$ GPa and $C_{44} = 2.175 \pm 0.023$ GPa. These values are consistent with BLS measurements by Halawith [20] on PMMA with a molecular weight of $\sim$200 kg mol^{-1}.
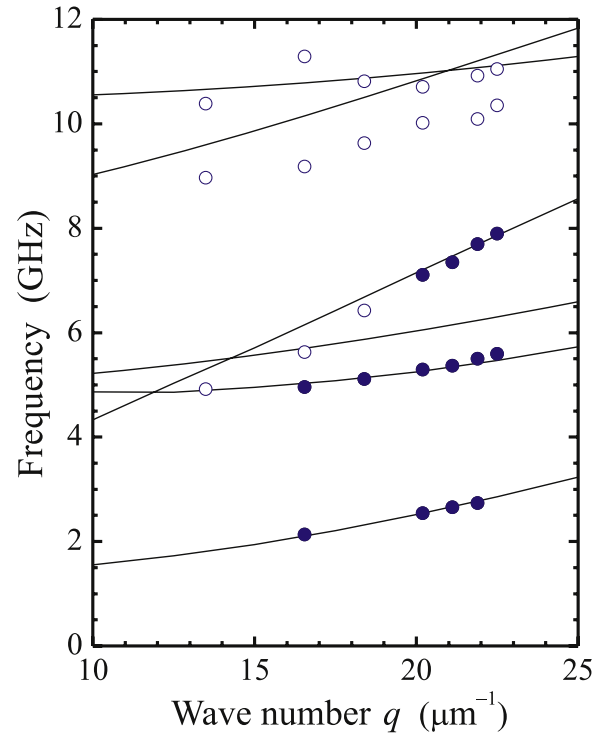

Figure 3. Symbols: measured acoustic frequencies versus corrected wavenumber q along the principal axis of the nanolines. Lines: calculated dispersion curves employing the values of C_{11}, C_{44}, and dimensional parameters w and h obtained by finite-element inversion analysis of the data points that are plotted as solid symbols.

4.2. Finite-element analysis

Inversion analysis of the measured dispersion data (figure 3) was performed with the nanoline dimensions and elastic stiffness coefficients C_{11} and C_{44} as adjustable parameters. The PMMA is assumed to be elastically isotropic. To maximize the robustness of this analysis, a simplified geometry is assumed, in which the number of dimensional parameters is limited to two: the height h and width w of the cross-sectional geometry shown in figure 4. The sides of the nanoline are approximated as vertical and parallel, and the top is approximated as semicircular. The additional complication of tilted sides, indicated in the CD-SAXS results of section 4.3, is not considered in the FE analysis. Following Heyliger *et al* [11], an 8×16 mesh is used for the rectangular region, and an additional 32 elements (8 circumferential divisions and 4 radial divisions) are used to represent the semicircular region.

The inversion analysis is limited to the lowest three measured dispersion curves in figure 3. These correspond to the sharpest peaks in the BLS spectra, with correspondingly lower uncertainties in the frequencies.

Heyliger *et al* [11] found that, to keep errors in the calculated frequencies below 1.8% with the approximate boundary conditions described in section 3.2, inversion analysis must be limited to values of hq greater than 1.0 for the Rayleigh-like mode and greater than 2.1 for the lowest Sezawa-like mode, when h is between 50 and 200 nm. Following these guidelines, we limit the analysis to the data points plotted as solid circles in figure 3. The range of valid data
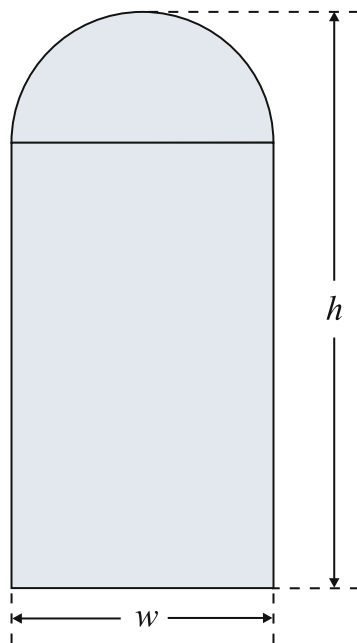
Figure 4. Shape and definitions of dimensional parameters used in the inversion analysis of BLS spectra.

Figure 5. Calculated displacement patterns for the four lowest-frequency modes with $k = 20\ \mu\text{m}^{-1}$. The frequencies increase in the order of the mode labeling from (i) to (iv).

to include for the flexural (lowest) mode is assumed to be at least as large as that for the Rayleigh-like (second) mode. This assumption is consistent with the close correspondence, over a relatively broad range of q, of finite-element and Farnell–Adler calculations of the flexural mode presented by Heyliger *et al* [11].

Before proceeding with the analysis, it is useful to consider the relative sensitivity of the vibrational frequencies to each of the four input parameters C_{11}, C_{44}, w, and h. Table 1 presents results of such an analysis as the ratio of fractional changes in frequency resulting from a given fractional change in each of the input parameters, where the frequencies of the lowest flexural, Rayleigh-like, and Sezawa-like modes are labeled f_1, f_2, and f_4, respectively (corresponding to the ordering of frequencies in the finite-element calculations, with f_1 being the lowest). For example, a change of 1% in the shear constant C_{44} leads to a fractional change of 0.46% in f_1. These calculations were performed at a wavenumber q of 20 μm^{-1}. The frequencies of this set of modes depend only weakly on C_{11}. Their much greater dependence on C_{44} is a reflection of the fact that each of these three modes involves predominantly shear displacements. The width has a strong influence on only the lowest of the three modes.

Since C_{11} has such a relatively small influence on the frequencies, its value was fixed during the initial stages of the analysis at the measured bulk value of 9.161 GPa. Also, to eliminate divergence of the fit from physically plausible values arising from the interplay of parameters, C_{44} and the dimensional parameters h and w were alternately fixed in an iterative approach during the analysis. After converging to a result under the constraint of fixed C_{11}, the analysis was refined by allowing C_{11} to vary along with the other three parameters. The values determined from this analysis are $C_{11} = 8.87 \pm$
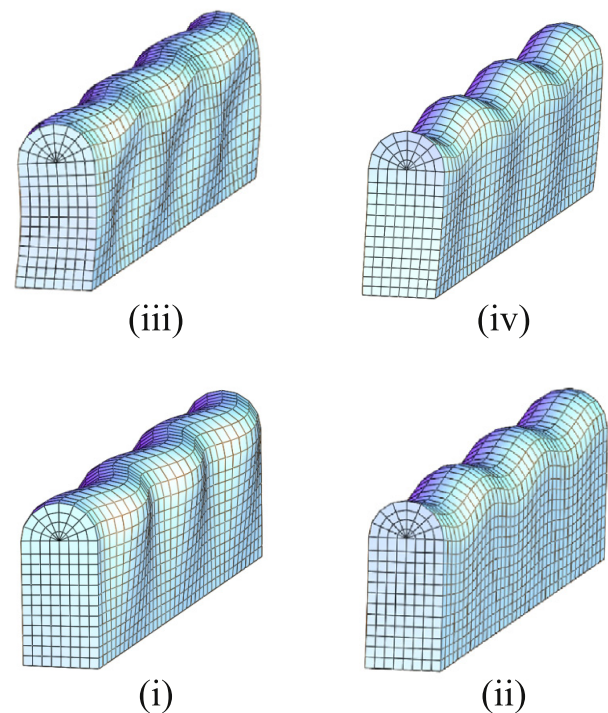
Table 1. Sensitivity of calculated frequencies of the lowest flexural, Rayleigh-like, and Sezawa-like modes (f_1, f_2, and f_4, respectively) on each of the four input parameters C_{11}, C_{44}, w, and h.

	$\Delta C_{11}/C_{11}$	$\Delta C_{44}/C_{44}$	$\Delta w/w$	$\Delta h/h$
$\Delta f_1/f_1$	0.04	0.46	0.60	0.56
$\Delta f_2/f_2$	0.06	0.44	0.00	0.70
$\Delta f_4/f_4$	0.06	0.44	0.02	0.18

0.27 GPa, $C_{44} = 1.92 \pm 0.06$ GPa, $w = 55.5 \pm 2$ nm, and $h = 122.1 \pm 4$ nm.

The dispersion curves below 12 GHz obtained from the inversion analysis are plotted in figure 3 along with the BLS data. The curves from the inversion are in close agreement with the data that are fit (the points plotted as solid symbols), with a standard deviation of 0.13 GHz. As in previous studies [7, 8], no evidence for the third calculated mode is present in the BLS measurements.

The corresponding three-dimensional displacement patterns for the four lowest-frequency modes with $q = 20\ \mu\text{m}^{-1}$ are shown in figure 5. These patterns are similar to those reported previously [11] for nanolines with a rectangular cross section. The lowest mode involves relatively simple transverse flexural vibrations. The second mode is Rayleigh-like, with primarily vertical displacements. The third mode is a higher-order flexural vibration, with greater vertical phase variation than the lowest flexural mode. This is the mode with a lower scattering cross section, being undetectable in the measured spectra. The fourth mode is the lowest-order Sezawa-
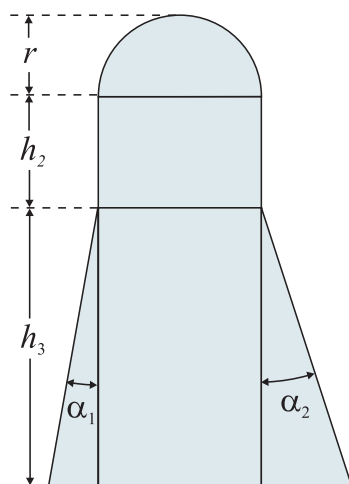
Figure 6. Shape and definitions of dimensional parameters used in the inversion analysis of CD-SAXS spectra.

like mode. The fifth and sixth modes (not shown in figure 5) are, respectively, higher-order Sezawa-like and flexural modes, similar to those previously reported by Heyliger *et al* [11] for nanolines with a rectangular cross section. However, the frequency ordering of these two modes at $q = 20 \ \mu m^{-1}$ in the rounded-top nanolines considered here is reversed relative to that in the rectangular nanolines considered by Heyliger *et al*.

4.3. CD-SAXS

CD-SAXS spectra were acquired over a range of angles from $-30°$ to $+30°$, where $0°$ is defined as incidence of the beam normal to the substrate. Inversion analysis of the CD-SAXS spectra was performed under the assumption of a cross-sectional geometry with the form shown in figure 6. The dimensional parameters determined from this analysis are $r = 22 \pm 2$ nm, $h_2 = 30 \pm 5$ nm, $h_3 = 75 \pm 5$ nm, $\alpha_1 = 10° \pm 2°$, and $\alpha_2 = 18° \pm 2°$.

5. Discussion

The overall dimensions of the nanolines determined from FE analysis of the BLS data are consistent with those determined from CD-SAXS. The average nanoline width (including the rounded upper section) from FE/BLS is 52.7 ± 3.8 nm, and that from CD-SAXS is 53.5 ± 4.9 nm. The total height from FE/BLS is 122.1 ± 4 nm, and that from CD-SAXS is 127 ± 7 nm.

The values obtained for C_{11} and C_{44} from the FE/BLS analysis are, respectively, 3.1% and 11.6% below the values that we determined for bulk PMMA made from the same starting material. No independent measurements are available for direct comparison with these results at gigahertz frequencies. However, Stafford *et al* [4] performed quasi-static buckling measurements of the in-plane modulus $\bar{E}$ (defined as $E/(1 - \nu^2)$, where E is Young's modulus and ν

is Poisson's ratio) of unannealed 184 kg mol^{-1} PMMA films with thicknesses in the range of 5–120 nm and found $\bar{E}$ to drop substantially in the lower half of this range. The method in that study involved measurements of the periodicity of buckling of the films subjected to uniaxial stress on a relatively soft elastic substrate [21]. The difference of the values reported by Stafford *et al* [4] for $\bar{E}$ for films with thicknesses of 82 and 46 nm is ∼9%, but this difference is within the uncertainty of the measurements. Linear interpolation of these values suggests that $\bar{E}$ for a thickness of ∼55.5 nm (the width that we determined for the nanolines in this study) may be on the order of 7% lower than that for a thickness of 82 nm.

We have performed more extensive buckling measurements with lower uncertainties on PMMA films with a molecular weight of 91 kg mol^{-1} that were annealed at a temperature 10 °C below the glass transition temperature. The values of $\bar{E}$ from these measurements are 3.49 ± 0.11 GPa, 3.93 ± 0.20 GPa and 3.96 ± 0.19 GPa for films with thicknesses of 55.6 nm, 132.8 nm and 200.7 nm, respectively. These values correspond to a fractional change in $\bar{E}$ of -0.115 ± 0.070 as the thickness is decreased to 55.6 nm from the range of 132–201 nm.

To enable a comparison of our BLS/FE results with these buckling measurements, we estimate Young's moduli from the values determined above for C_{11} and C_{44} using the relation, valid under the assumption of elastic isotropy, of

$$E = \frac{(3C_{11} - 4C_{44})C_{44}}{C_{11} - C_{44}}. \quad (2)$$

E is found to be 5.85 ± 0.09 GPa for bulk PMMA and 5.24 ± 0.35 GPa for the nanolines. The corresponding fractional drop in E of the nanolines, relative to bulk PMMA, is 0.104 (10.4%), with an uncertainty of ± 0.06. This value is consistent with our buckling measurements on 91 kg mol^{-1} PMMA and with the earlier results of Stafford *et al* [4].

Although this comparison with buckling results supports the credibility of our BLS/FE results for the stiffness coefficients, one should note the significant differences in methods, materials, and geometry. The modulus determined in buckling measurements is the 'relaxed' modulus, involving substantial viscoelastic and/or anelastic reductions in stiffness relative to the hypersonic modulus determined using BLS/FE. Therefore, if the viscoelastic or anelastic response of the material is dependent on size, this will more strongly affect the thickness dependence of the modulus determined from buckling measurements than that determined from BLS measurements. The differences in molecular weight are also significant. However, the results of Stafford *et al* [4] on polystyrene suggest that size-dependent effects on the modulus have little dependence on the molecular weight. Finally, note that the geometry of the imprinted nanolines is very different from that of a film on a substrate. One may expect the greater surface-to-volume ratio of nanolines relative to a blanket film of the same thickness to lead to a relatively greater size dependence of the elastic stiffness coefficients.

With respect to previous experimental studies, one should also note the work of Stoykovich *et al* [2] on the dimensional dependence of the quasi-static Young's modulus in PMMA (∼950 kg mol^{-1}). Stoykovich *et al* used a technique involving

the application of capillary forces between lithographically patterned PMMA nanobeams. They found the modulus to drop rapidly below the bulk value when the beam thickness dropped below $\sim$115 nm, reaching $\sim$1/3 of the bulk value at $\sim$75 nm (a much more rapid drop than that determined from our buckling measurements and that reported by Stafford *et al* [4]). However, they suggest that electron beam damage or plasticization of the polymer during fabrication may contribute substantially to the apparent dependence on beam dimensions in their measurements.

Previous BLS studies of polymeric membranes and films on substrates have not found evidence for thickness-dependent effects on the C_{ij}. Forrest *et al* [22] found no thickness dependence in polystyrene membranes with thicknesses in the range of 29–190 nm. However, considering the differences in materials and geometry, this result is not inconsistent with the results that we present here. In particular, note that the buckling results of Stafford *et al* [4] indicate that size-dependent effects on the modulus become significant at lower thicknesses in polystyrene than in PMMA; they found no evidence for such effects in polystyrene with thicknesses greater than $\sim$40 nm. Cheng *et al* [23] performed BLS measurements on PMMA films with a molecular weight of 62 kg mol^{-1} on glass substrates. They found C_{11} and C_{44} in 41 nm films to be, respectively, 8% higher and 8% lower than values of the stiffness coefficients of 492 nm films, but considered this difference to be within the margin of uncertainty of the measurements and analysis. Hartschuh *et al* [7] also found no evidence for size-dependent effects on elastic stiffness coefficients in photolithographically patterned nanolines of a commercial photoresist with nanoline widths as small as 88 nm; these results also are not inconsistent with results presented here, considering the differences in materials and the larger dimensions. Therefore, although no previous BLS studies have found evidence for dimensional dependence of elastic constants in polymers, we consider none of these studies to be inconsistent with the results presented here.

One additional feature of figure 3 that should be noted is the relatively poor correspondence of the calculated dispersion curve of the second Sezawa-like mode (extending from 9 to 11.8 GHz) with the BLS data. As indicated above, this curve was not included in the inversion analysis. We suggest that inaccuracy in predicting the frequencies of this mode arises from inaccuracy in the assumed form of the cross-sectional geometry. This hypothesis is supported by preliminary FE calculations (not shown) for nanolines with a tapered base, which show a relative downward shift of the frequencies of this mode.

6. Conclusions

The results presented here provide the first evidence of size-dependent effects on elasticity of polymers determined from BLS measurements. The values of parameters determined from the inversion analysis of BLS spectra are found to be credible with respect to both the stiffness coefficients (C_{11} and C_{44}) and the dimensional parameters (w and h), based on

comparisons with CD-SAXS measurements of the nanolines and elastic buckling measurements of PMMA films. The fact that such results have been obtained from nanolines with a less than simple cross-sectional geometry suggests that the BLS/FE inversion approach is fairly robust in its determination of the C_{ij} and overall dimensions, even when simplifying approximations are made for the cross-sectional shape.

With respect to potential directions of future studies with BLS/FE, it is intriguing to speculate about the level of accuracy in the determination of C_{ij} that might be achievable from analysis of BLS measurements for nanolines with more regular specified forms of the cross-sectional geometry, which are becoming more achievable as nanoimprinting techniques advance. In particular, since the flexural modes of nanolines involve a different polarization of shear displacements than the Rayleigh-like and Sezawa-like modes, higher-accuracy inversion analysis of BLS data might enable a determination of elastic anisotropy, which must be understood and quantified for accurate modeling of imprinting processes. One can expect elastic anisotropy to occur, at some length scale, whenever the height and width of nanolines are unequal.

References

[1] Guo L J 2004 *J. Phys. D: Appl. Phys.* **37** R123
[2] Stoykovich M P, Yoshimoto K and Nealey P F 2008 *Appl. Phys.* A **90** 277
[3] Van Workum K and de Pablo J J 2003 *Nano Lett.* **3** 1405
[4] Stafford C M, Vogt B D, Harrison C, Julthongpiput D and Huang R 2006 *Macromolecules* **39** 5095
[5] Mutti P, Bottani C E, Ghislotti G, Beghi M, Briggs G A D and Sandercock J R 1995 *Advances in Acoustic Microscopy* vol 1, ed A Briggs (New York: Plenum) p 249
[6] Hartschuh R, Ding Y, Roh J H, Kisliuk A, Sokolov A P, Soles C L, Jones R L, Hu T J, Wu W L and Mahorowala A P 2004 *J. Polym. Sci.* B **42** 1106
[7] Hartschuh R D, Kisliuk A, Novikov V, Sokolov A P, Heyliger P R, Flannery C M, Johnson W L, Soles C L and Wu W L 2005 *Appl. Phys. Lett.* **87** 173121
[8] Johnson W L, Flannery C M, Kim S A, Geiss R, Heyliger P R, Soles C L, Hu W and Pang S W 2006 *Mater. Res. Soc. Symp. Proc.* **924** Z08–31
[9] Farnell G and Adler E 1972 *Physical Acoustics* vol 9, ed W P Mason and N Thurston (New York: Academic) p 35
[10] Auld B A 1990 *Acoustic Fields and Waves in Solids* vol 2 (Malabar, FL: Krieger)
[11] Heyliger P R, Flannery C M and Johnson W L 2008 *Nanotechnology* **19** 145707
[12] Chen L J, Lin S W, Gau T S and Lin B J 2003 *Proc. SPIE* **5038** 166
[13] Nikitin A V, Sicignano A, Yeremin D Y, Sandy M and Goldburt T 2003 *Proc. SPIE* **5038** 651
[14] Sandercock J R 1982 *Light Scattering in Solids III* (*Topics in Applied Physics* vol 51) ed M Cardona and G Guntherodt (Berlin: Springer) p 173
[15] Stoddart P R, Crowhurst J C, Every A G and Comins J D 1998 *J. Opt. Soc. Am.* B **15** 2481
[16] Wang C Q, Jones R L, Lin E K, Wu W L, Rice B J, Choi K W, Thompson G, Weigand S J and Keane D T 2007 *J. Appl. Phys.* **102** 024901

[17] Wang C Q, Jones R L, Lin E K, Wu W L and Leu J 2007 *Appl. Phys. Lett.* **90** 193122

[18] Jones R L, Hu T, Lin E K, Wu W L, Kolb R, Casa D M, Bolton P J and Barclay G G 2003 *Appl. Phys. Lett.* **83** 4059

[19] Prasciolu M, Candeloro P, Kumar R, Businaro L, Di Fabrizio E, Cojoc D, Cabrini S, Liberale C and Degiorgio V 2003 *Japan. J. Appl. Phys.* **42** 4177

[20] Halawith B 1982 *J, Polym. Sci. Pol. Lett.* **20** 583

[21] Stafford C M, Harrison C, Beers K L, Karim A, Amis E J, VanLandingham M R, Kim H C, Volksen W, Miller R D and Simonyi E E 2004 *Nat. Mater.* **3** 545

[22] Forrest J A, Dalnoki-Veress K and Dutcher J R 1998 *Phys. Rev. E* **58** 6109

[23] Cheng W, Sainidou R, Burgardt P, Stefanou N, Kiyanova A, Efremov M, Fytas G and Nealey P F 2007 *Macromolecules* **40** 7283